Atmospheric Environment 295 (2023) 119556

Contents lists available at ScienceDirect

Atmospheric Environment

journal homepage: www.elsevier.com/locate/atmosenv

Tracking sources of PM_{10} emissions and deposition in the industrial city of Ostrava, Czech Republic: A carbonaceous $\delta^{13}C$-based approach

Frantisek Buzek [a,*], Bohuslava Cejkova [a], Ivana Jackova [a], Radim Seibert [b], Jan Curik [a], Frantisek Veselovsky [a], Daniel A. Petrash [a]

[a] Czech Geological Survey, Geologicka 6, 152 00, Prague 5, Czech Republic
[b] Czech Hydrometeorological Institute, K Myslivne 2182/3, 708 00, Ostrava-Poruba, Czech Republic

HIGHLIGHTS

- Sources of particulate matter emissions were traced using ^{13}C data of organic and black carbon.
- Studied area is the industrial city area with numerous pollution sources.
- The apportionment of sources was calculated from the mass balance of organic carbon and ^{13}C.
- Deposition of emissions was detected in ^{13}C of black carbon on surface layer of soils.

GRAPHICAL ABSTRACT

Apportionment of OC sources in PM_{10} emissions in Ostrava 2021 at S wind conditions

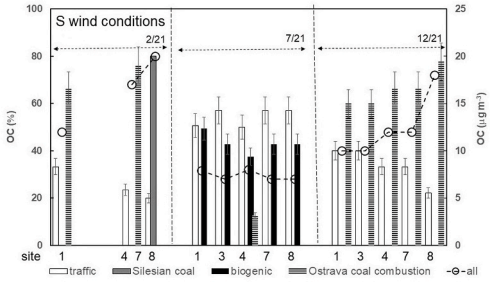

ARTICLE INFO

Keywords:
Black carbon
Organic carbon
Carbon isotope composition
Particulate matter emission

ABSTRACT

The sources of airborne particulate matter (PM_{10}) emissions in Ostrava, Czech Republic, were investigated. Emphasis was placed on their organic carbon (OC) and elemental carbon (EC) contents, and their carbon stable isotope composition, $\delta^{13}C$. Emission sources were identified using OC-$\delta^{13}C$ and concentration values. To track the extent of long-term deposition, these sources were also identified using the black carbon (BC) $\delta^{13}C$ values of soil samples. At all sampling sites, wind flow is predominantly (65–80%) bidirectional in either SW-NE or NE-SW trajectories. Source apportionment along these dominant airflow trajectories was calculated from an isotopic ^{13}C mass balance, and according to differences in the OC content and $\delta^{13}C$ values of PM_{10}. Determined emission sources are: (i) combustion of Silesian hard coal ($\delta^{13}C = -24.5‰$); (ii) local Ostrava coal combustion ($\delta^{13}C = -25.5$ to $-26‰$), automotive emissions ($\delta^{13}C = -26.5‰$), and biogenic particles ($\delta^{13}C = -28$ to $-28.5‰$). Winter emissions (mean OC concentrations from 12 to 25 μg m^{-3}) originated mostly from coal combustion (80%) in domestic and industrial point sources. Differences were ascribed to automotive emissions. Ostrava is located near the Czech-Polish border, transboundary emissions are transported under a southbound wind flow that transported from 40 to 80% of the collected PM_{10}. Summer emissions were lower (mean OC concentration from 6 to 8 μg m^{-3}). Automotive emissions accounted for up to 40%, whilst biogenic production accounted for 60%. Absence of ^{13}C isotope data of secondary OC (SOC 1.2–1.5 μg m^{-3}) increases uncertainty in our source apportionment in summer; when SOC could comprise >20% of total OC. Contribution of SOC to the winter-measured

* Corresponding author.
E-mail addresses: frantisek.buzek@geology.cz (F. Buzek), bohuslava.cejkova@geology.cz (B. Cejkova), ivana.jackova@geology.cz (I. Jackova), radim.seibert@chmi.cz (R. Seibert), jan.curik@geology.cz (J. Curik), frantisek.veselovsky@geology.cz (F. Veselovsky), daniel.petrash@geology.cz (D.A. Petrash).

https://doi.org/10.1016/j.atmosenv.2022.119556
Received 22 September 2022; Received in revised form 12 December 2022; Accepted 13 December 2022
Available online 19 December 2022

OC is much lower (5–10%), and has no significant effect on mass balances. The upper soil layer analyses revealed long-term deposition of the same emissions sources. We conclude that the stable $\delta^{13}C$ isotope values of OC and EC are useful for discriminating against local sources of PM_{10} pollution in relatively small urban areas, containing discrete polluting sources. Such a simplified approach can be easily standardized and implemented to manage regulatory compliances in the increasingly commoditized carbon offset market.

1. Introduction

Carbonaceous particles constitute a significant part of particulate matter (PM) emissions. Although carbonaceous particles represent a low percentage of all aerosols (Klimont et al., 2017), their sources and distributions have received the most attention because of their sorption capacity for volatile organic carbon and other dangerous (cancerogenic) volatiles (Chow et al., 2010); and their role catalyzing aerosol reactions (He et al., 2018). The total carbon (TC) of carbonaceous particles is made up of a variety of compounds, including organic carbon (OC), elemental carbon (EC), and inorganic carbon (IC) particles. OC and EC account for the largest proportion. Primary OC originates from the combustion of fossil fuels and biogenic sources. Secondary OC (SOC) is produced during atmospheric reactions of gaseous organic compounds (Jones and Harrison, 2005). Most SOC is water soluble (WSOC). WSOC is reactive, it increases the condensation of aerosol particles (Asa-Awuku et al., 2011) and promotes OC dispersion via wet deposition. EC, also called black carbon (BC), is derived from primary emission sources via combustion of several types of organic matter. The IC components of carbonaceous particles are carbonates from soil dust.

Sources of OC and EC can be differentiated by their stable isotope carbon compositions ($\delta^{13}C$) (Dienes, 1980; Widory, 2006). Due to the high stability, low reactivity, and direct link of EC with combustion processes, EC is more commonly used to trace the origin of carbon in PM than OC. Yet, most combustible products (coal, oil, gas, wood, and biogenic material) have characteristic $\delta^{13}C$ values of OC, and the assignment of atmospheric pollution sources based on the $\delta^{13}C$ signature of OC is straightforward. PM_{10} includes particles less than 10 μm in diameter. PM_{10} is a mixture of different particles derived from various sources, and its partitioning changes with time, season, wind direction, and climate. The identification of carbonaceous PM_{10} sources could thus be hampered by $\delta^{13}C$ overlaps resulting from admixture of various particulates with multiple $\delta^{13}C$ signatures. This complexity needs to be handled in combination with other variables useful for specifying multiple single sources.

The contribution of fossil and biogenic fuels to PM pollution has been evaluated from $\delta^{13}C$ and $\Delta^{14}C$ data, as recent organic matter has ^{14}C radioactivity (Szidat et al., 2004; Garbariene et al., 2016; Liu et al., 2018; Zimnoch et al., 2020). The seasonal differences in concentrations of OC and EC, in combination with their $\delta^{13}C$ values, have been used to identify PM sources from winter and summer emissions (Cao et al., 2011; Morera-Gomez et al., 2021). For instance, seasonal variations in $\delta^{13}C$ of PM were used to identify sources of emissions in Mexico City (Lopez-Veneroni, 2009). Differences between the $\delta^{13}C$ values of PM and TC, OC and EC concentrations during winter and spring (i.e., vegetation growth period) enabled distinguishing the sources of local emissions in a recently conducted study in Lower Silesia, Poland (Gorka et al., 2020).

Here we identify sources of PM emissions in the industrial city of Ostrava, Czech Republic. By air sampling at discrete sites, the contributions of these emissions to total emissions during the year were estimated via isotope ratio mass spectrometry. Our study looks at the establishment of a monitoring mechanism to track local pollution emitters in areas affected by transboundary transport of organic C-bearing PM_{10}. This is though important for standardization aimed at regulation of the carbon offset market, and for evaluating manageable levels of uncertainty in emission monitoring practice involving different market participants including state regulators and regulated stakeholders.

2. Materials and methods

2.1. Site description

For more than 100 years, Ostrava city (current population *ca.* 280,000 inhabitants; area: 214 km^2) has been at the center of one of the most heavily industrialized areas in Central Europe. According to recent research work, Ostrava is the most polluted urban area in the Czech Republic (Jancik et al., 2013), and the Ostrava district together with the neighboring voivodeship (province) of Lower Silesia (Poland) are amongst the most polluted central European regions. Katowice, the industrial center of Lower Silesia, and Ostrava are both close to the border, and are about 70 km apart. There is recurrent trans-border transport of pollutants from the Czech Republic to Poland, and vice versa. Fig. 1 shows the location of Ostrava and the position of our sampling points in the study area. It also shows the wind trajectories, predominantly in either northern to northeastern or southern to southwestern directions (65–80% of the time). Local sources of PM_{10} emissions in the study area include iron works, coke production, smelters, coal combustion in both central heating and domestic heating appliances and large traffic volumes (cars and trucks) (Jancik et al., 2013).

2.2. Sample preparation, analyses and instrumentation

During the period February–December 2021, atmospheric aerosol particles PM_{10} emissions (2.5 μm ≤ particulate diameter ≤10 μm) were sampled at five sampling locations (Fig. 1). Adjacent soil samples were collected to determine long-term PM_{10} deposition. PM_{10} samples were collected, using an automatic high-volume sampling device (Leckel SEQ47/50-RV, Sven Leckel, Berlin, Germany) on pre-combusted (4 h at 450 °C) quartz filters (Whatman QF, diameter: 47 mm). The filters were conditioned (before and after sampling) in a desiccator at 22 °C. The sampling airflow was about 55 m^3 per 24 h. Samples were collected for 30 consecutive days from three sites during February, two additional sites were added in July and December. Samples collected during a temperature inversion ($PM_{10} > 50$ μg m^{-3}) were analyzed separately from other samples. In total, we analyzed the OC and EC contents, and OC and EC $\delta^{13}C$ values of more than 400 samples.

The filters collected from the sampling apparatus were fumigated with reagent grade hydrochloric acid (HCl; Komada et al., 2008) to remove possible carbonate IC. Pre-weighted punches of exposed filters (1 cm^2) were dampened with distilled water; placed in silver capsules, and left overnight to further react with concentrated HCl. Capsules were then dried at 40 °C, weighed, and measured for their OC content in an elemental analyzer (Fisons 1108, Thermo-Scientific). To remove OC prior to measuring EC contents, the filters were combusted for 16 h at 375 °C (Gustafsson et al., 2001). The weight of the filtrates were determined by subtracting the weight of blank filters. Precision of the carbon content determinations was better than 0.1 wt %.

The $\delta^{13}C$ of OC and EC in the filters was measured by combustion in the elemental analyzer previously described, coupled on-line to an isotope ratio mass spectrometer (IR-MS) with a ConFlo IV reference gas unit (Delta V, Thermo-Scientific). The reproducibility of the $\delta^{13}C$ measurements (better than 0.1‰) was checked by measuring NBS-22 reference material ($\delta^{13}C = -30.06$‰; National Bureau of Standards, USA) at every sixth sample. We analyzed the OC and EC concentration data from the sampling sites separately by the thermo-optical method, according to the protocol of the European Supersites for Atmospheric

Aerosol Research (EUSAAR, Cavalli et al., 2010). WSOC was analyzed by ion chromatography (CHMI et al., 2022). Wind direction, wind speed (at 10 m height), and other weather parameters such as air humidity and temperature were retrieved from historical records (available at https://www.in-pocasi.cz/archiv/archiv.php?historie=2021-02-17&region=6)

For the measurement of soil OC, BC, and their $\delta^{13}C$ values, about 500 g of non-cultivated soil was collected from the surface layer down to 5 cm; plant debris, stones, and soil agglomerates (>2 mm) were separated manually. Triplicates were collected from each sampling site. The soil was homogenized (particle sizes <0.06 mm), and the carbonate fraction (IC) was removed by fumigation with HCl. The OC fraction was determined by combustion of 10–15 mg of soil in the elemental analyzer; with acetanilide as reference material. Reproducibility was better than 0.1%. The $\delta^{13}C$ of OC in soil was determined on the IR-MS described above, with the ConFlo IV reference gas unit. The BC fraction in soil and its $\delta^{13}C$ value were determined similarly to our filtrate OC fractions, but the soil samples were preheated for 16 h at 375 °C.

For comparison purposes, isotopic $\delta^{13}C$ compositions of coal samples were retrieved from the literature. Diesel and gasoline soot were collected directly from the deposit of vehicle exhaust pipes (12 samples) and analyzed for OC contents and $\delta^{13}C$ values in the same way as QF filters. $\delta^{13}C$ data measured on QF filters retrieved from a tunnel in Prague (not published data 2019) recorded similar $\delta^{13}C$ values (−26.7 ± 0.3‰).

2.3. Mass balance calculations

The source mixing equation was applied to verify source mixing (coal combustion, biogenic inputs, and automotive inputs). For this purpose, we parametrically solved equations (1) and (2):

$$C_{tot} = C_{coal} + C_{bio} + C_{traf,} \quad (1)$$

$$C_{tot} * \delta_{tot} = C_{coal} * \delta_{coal} + C_{bio} * \delta_{bio} + C_{traf} * \delta_{traf,} \quad (2)$$

where C_{tot}, C_{coal}, C_{bio}, and C_{traf} are the masses of all carbon particles, carbon from coal combustion, biogenic sources, and traffic inputs in the form of diesel and gasoline combustion, and δ_{tot} δ_{coal} δ_{bio} and δ_{traf} are their respective $\delta^{13}C$ values.

To determine the contributions of single components (e.g., traffic inputs C_{traf}), the $\delta^{13}C$ values of all inputs must be known, together with the mass relationships between C_{tot}, C_{coal} and C_{bio}. The two linear equations with three variables can be solved in the form of a linear combination of variables, when it is possible to simplify all of the coefficients of linear factors to numbers that are algebraically added to each other by using at most one coefficient. That coefficient determines the parametric solution, if any exists, of the equations (i.e., C_{tot}). A reduction in the number of variables can significantly help. For example, in summer, the contribution of coal combustion in domestic heating appliances needs no consideration, and only two contributors C_{traf} and C_{bio} must be included in the mass balance (Eqs. (1) and (2)).

A Keeling plot (Keeling, 1961) can be used in cases where there are only two sources of emissions in a given area, where one is the dominant source and the other non-dominant (i.e., background). In such cases, a simplified solution of Eqs. (1) and (2) can be simply obtained:

$$C_{tot} = C_{atm} + C_s \quad (3)$$

$$C_{tot} * \delta_{tot} = C_{atm} * \delta_{atm} + C_s * \delta_s \quad (4)$$

where C_{atm} and C_s are the masses of background atmospheric emissions and the emission source of interest, and δ_{atm} and δ_s are their corresponding $\delta^{13}C$ values. After approximation of carbon mass "C" by OC concentration "c", we obtained the atmospheric δ_{tot} relation in Eq. (5):

$$\delta_{tot} = c_{atm} * (\delta_{atm} - \delta_s) * 1/c_{tot} + \delta_s \quad (5)$$

As shown in Eq. (5), the relationship between δ_{tot} and c_{tot} is linear, with a slope of $c_{atm} * (\delta_{atm} - \delta_s)$ and has its intercept at the source δ_s value.

There are two basic assumptions underlying the Keeling plot method: (i) a system consists only of two reservoirs: the background and the source; and (ii) the isotopic ratio of the source carbon does not change during the observation time. Both assumptions are rarely fulfilled,

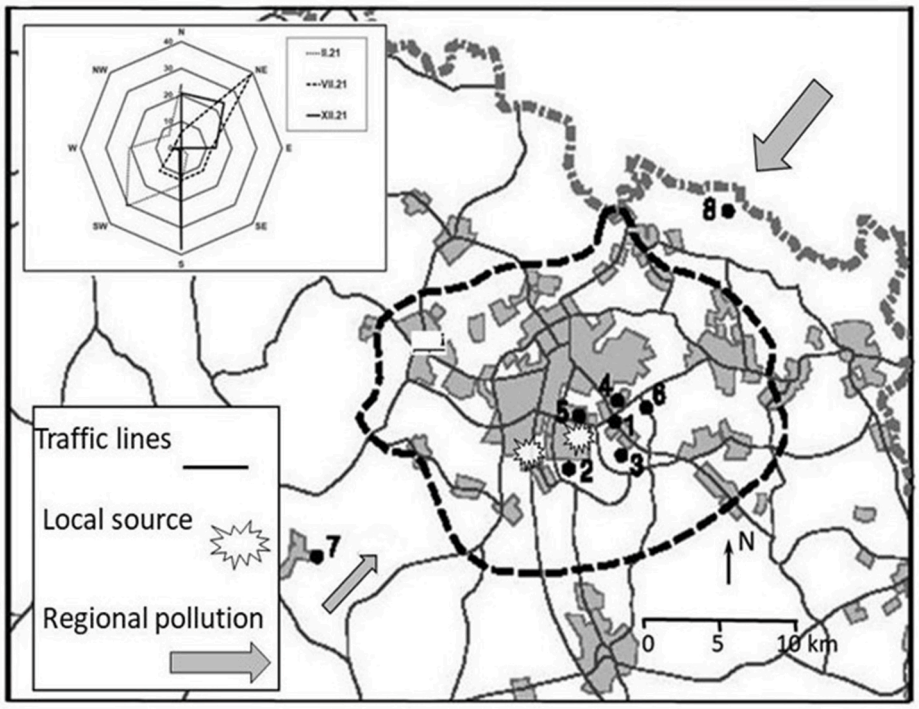

Fig. 1. The Ostrava area. Numbers 1–8 represent the sampling sites for atmosphere and soil collection. The flash symbols indicate local pollution sources, arrows correspond with regional pollution. The wind rose represents the wind directions during the three sampling periods in 2021.

especially in cases where multiple minor sources constitute the background, or when the carbon isotopic ratio of emitted particles can vary considerably through a sampling site. Nonetheless, the $\delta^{13}C$ of the dominant source can still be estimated using the Keeling plot method.

3. Results and discussion

3.1. Data analysis and statistics

Fig. 2 presents the mean OC concentrations and their corresponding $\delta^{13}C$ values, determined against a range of relevant qualitative (explanatory) variables, i.e., time of sampling, site, wind direction (azimuth) and wind speed. According to Fig. 2, the mean OC concentration differed considerably during winter and summer, with maximal and minimal mean values at sites 8 and 7 (20 and 10 μg m^{-3}, see also Fig. 1), and predominant wind azimuths centered at about 270 and 45°. The highest mean OC concentrations (34 μg m-3) were measured at the lowest wind speeds (between 2 and 4 km h-1). The $\delta^{13}C$ values of OC followed a trend as described by OC concentrations. Winter and summer sampling differed >2‰; extreme mean values were measured on sites 8 and 7. Lowest wind speeds corresponded with less negative δ13C values up to −24.4 ± 0.15‰.

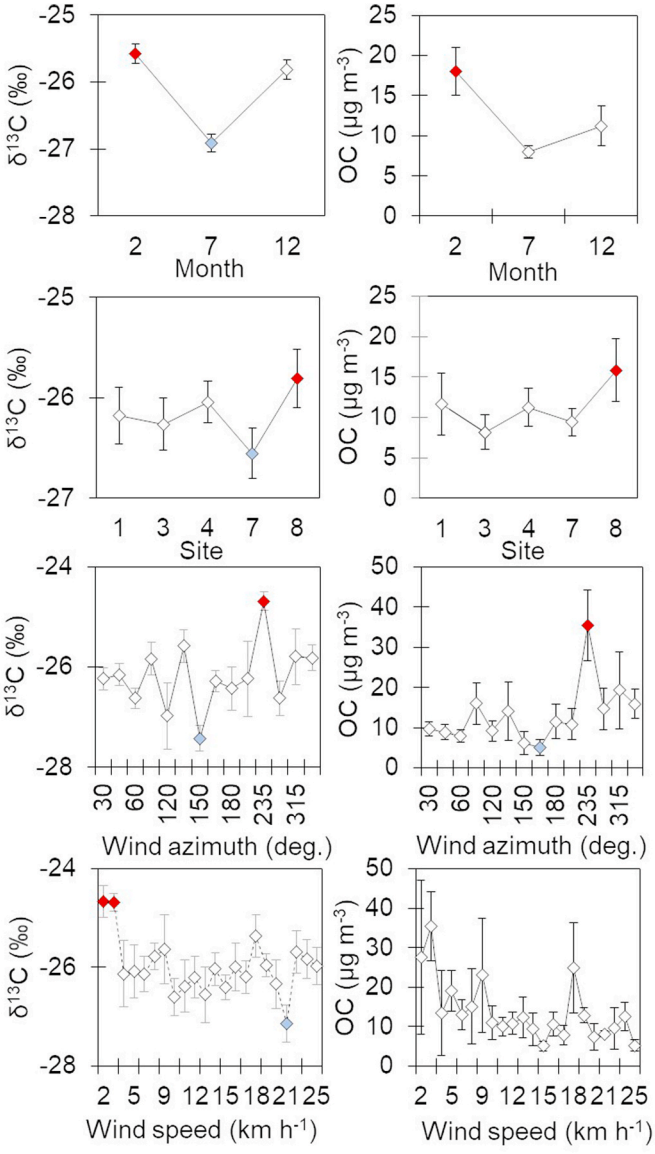

Fig. 2. Mean OC concentration and OC $\delta^{13}C$ values ± SE plotted against time of sampling, sampling site position, wind azimuth (wind direction) and wind speed. Extreme values are highlighted.

Supplementary Table SM1 presents descriptive statistics on measured OC concentration and $\delta^{13}C$ values. The approach applied for furthering statistical data mining is also detailed in the Supplementary Material. We implemented multiple 1-way ANalyses Of VAriance (ANOVA) to assess the significance of the studied qualitative over the variance of our quantitative parameters $\delta^{13}C$ and OC. To better constrain the role of each of the qualitative explanatory factors, we also used information from a two-way ANOVA, conducted separately to assess interactions of each of the explanatory variables of our model. This permitted weighting their influence as a combined source of variation in the variance partition.

Results from both statistical approaches are compiled in Table 1. The coefficients of determination of the model (0.743 for $\delta^{13}C$, and 0.536 for OC) provide a fair idea of the extent to which the variability of the modeled variables is explained by the explanatory variables: site, wind azimuth and speed, sampling month (Table 1). Accordingly, our statistical model confidently (α = 0.025) explained between ~74 and ~54% of variability of the dependent variables $\delta^{13}C$ and OC, respectively. The remaining percentage corresponds to hidden variables that could be classified as "random effects", for example site topography, unscheduled maintenance at polluting sources, storms, or commonly unidentified climatic phenomena, for example short-lived temperature inversions. Given that the probability corresponding to the Fisher's F is in all cases <0.0001 (Table 1), we can conclude that the explanatory variables considered have a significant combined effect on the variance of the dependent variables (see also Table SM 1 in Supplement). The explanatory variable "wind speed" appears to be the most influential over the dependent variable OC, for all the combined observations (i.e., regionally), the wind azimuth appears most relevant for $\delta^{13}C$ (Table 1, Supplementary Excel Sheet).

3.2. Identification of $\delta^{13}C$ of PM_{10} emitters

Atmospheric carbon emissions vary throughout the year. Yet, the individual contribution of some sources (e.g., industrial production and automotive emissions) remains nearly constant. Other sources are rather seasonal (i.e., coal combustion in local heating during winter, release of biogenic particles during the summer). To identify seasonal differences in emission sources, Fig. 3 displays histograms of $\delta^{13}C$ values of PM_{10} during our three sampling campaigns. Samples collected in February included marginal point sources at the study area, i.e., site 8 at the northern extreme, site 7 at the southern one; site 4 is inside the area, and close to local industrial sources of pollution (Fig. 1).

We applied the Keeling approach for each site to estimate a probable

Table 1
Summary outputs of a 3-way (bold), and discrete 1-way analyses of variance, computed against model Y = Mean(Y) with a significance level α = 0.025, p < 0.0001 (Pr > F).

		$\delta^{13}C$	OC′	Wilk's λ
Model	***F***	20.147	8.646	NA
	Adjusted[a] R^2	0.743	0.536	NA
Month	*F*	84.407	12.780	0.008
	R^2	0.465	0.109	
Site	*F*	5.743	0.024	0.076
	R^2	0.069	2.577	
Wind azimuth	*F*	4.608	6.187	0.030
	R^2	0.196	0.260	
Wind speed	*F*	3.414	5.005	0.037
	R^2	0.209	0.305	

[a] The adjustment represents the percentage of variance in the target field that is explained by the variable combination (model).

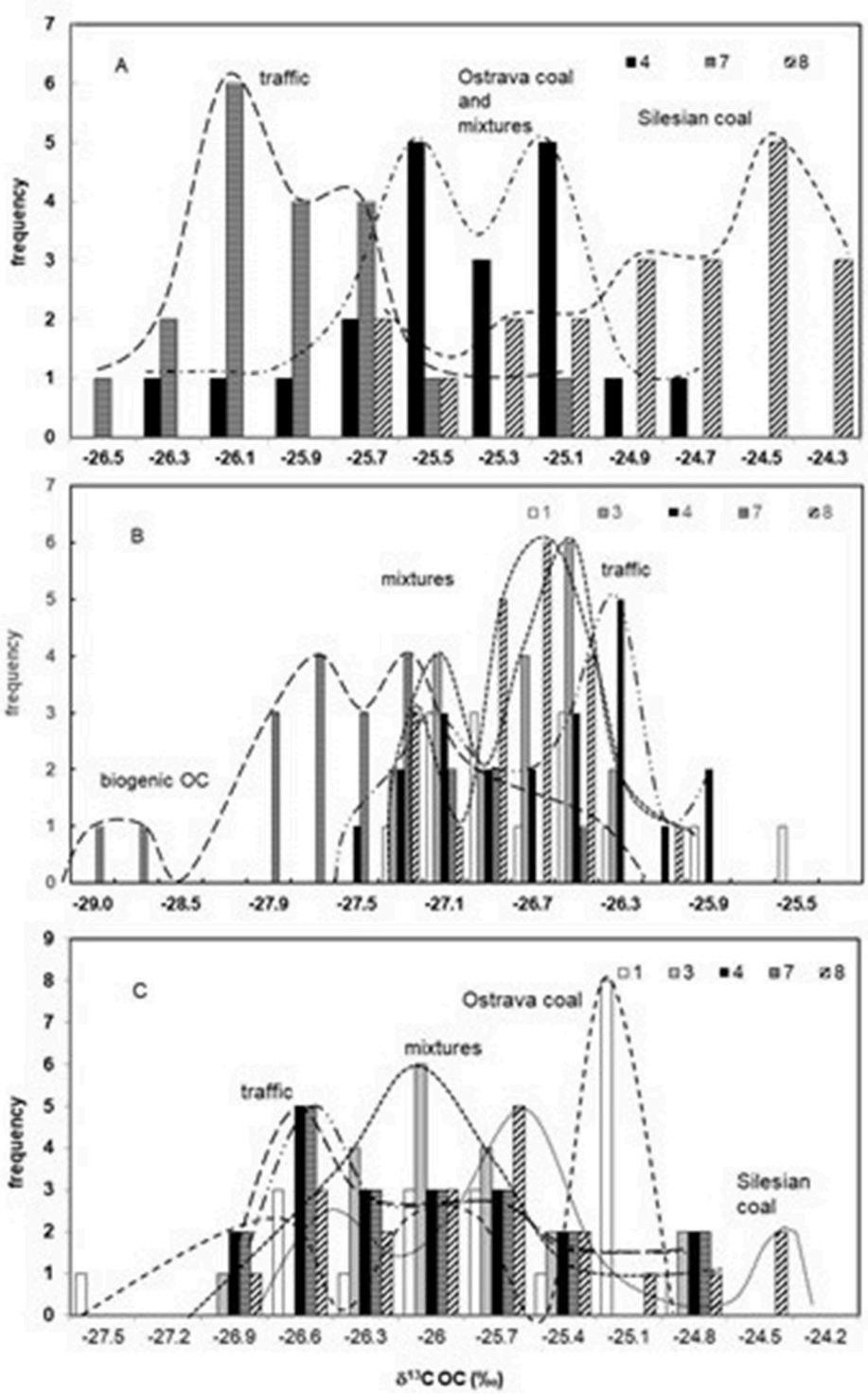

Fig. 3. Multimodal histograms of $\delta^{13}C$ values of OC in PM samples collected in February (A), July (B) and December 2021 (C). Probable emission sources are highlighted at frequency maxima.

$\delta^{13}C$ value of the emission source (Fig. S1 at the Supplement). A comparison of data plotted in Fig. 3A and Fig. S1 for the three sites, shows that the observed maxima and extrapolated values are in good agreement. In the first approximation, we took a $\delta^{13}C$ value of −24.5 as the source value for site 8, -25.9 or −26‰ for site 7, and -25.3 or −25.5‰ as the source $\delta^{13}C$ value inside the monitored area (site 4).

The high proportion of the bidirectional wind flow S to N and/or N to S (for 60–80% of measurements) simplified tracing the local pollution sources. The effect of the wind direction on OC concentration and $\delta^{13}C$ values is presented on data from our February sampling (Fig. 4).

The influence of the predominant wind directions on OC concentration and its $\delta^{13}C$ is strong. N winds brought high concentrations of OC (around 30 μg m^{-3}) from the Polish border. Their mean $\delta^{13}C$ values, −24.5 ± 0.2‰, are close to the known signature $\delta^{13}C$ of Silesian hard coal (Lewan and Kotarba, 2014; Zimnoch et al., 2020). Captured PM_{10} emissions were lowest at site 7 when the wind direction was from the south (southwest) towards the north (northeast) –from 5 to 15 μg m^{-3}, and exhibited $\delta^{13}C$ values ranging between −26.0 and −26.3‰. This

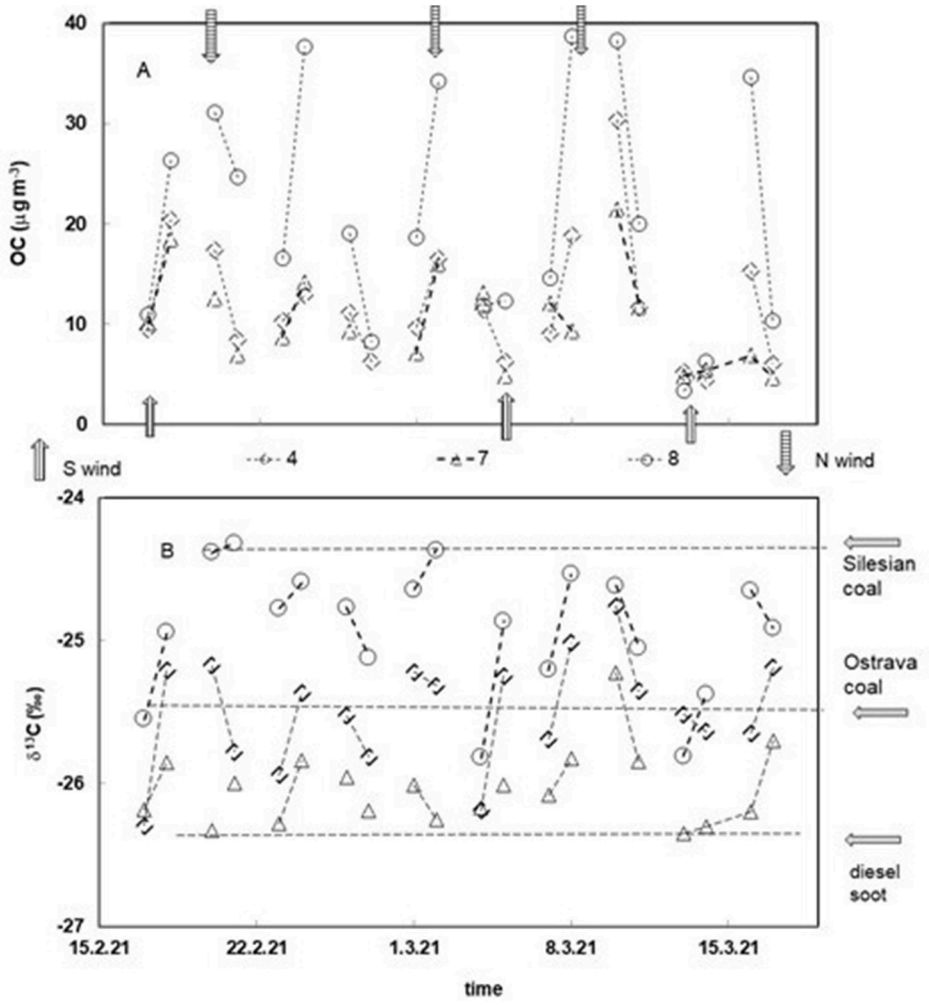

Fig. 4. Time plot of OC content in PM_{10} of sampled air (A) and $\delta^{13}C$ values (B) during the February sampling period. The vertical arrows show the days with a strong northern or southern wind. The horizontal arrows show the $\delta^{13}C$ values corresponding to probable sources.

narrow range is close to the values of diesel soot sampled from car exhausts (mean $\delta^{13}C$ value = −26.5 ± 0.2‰). Site 4 was characterized by a high concentration of OC in PM_{10} emissions (from 15 to 30 μg m^{-3}), with δ ^{13}C between −25.2 and −26‰ corresponding to the $\delta^{13}C$ values for either the local hard coal (δ ^{13}C = −25.5 to −25.8‰), or subbituminous coal transported from the Most basin (from −25.5 to −26.0‰; Buzek et al., 2022).

Table SM2 compiles the monthly mean $\delta^{13}C$ values and concentration of OC and EC on our sites calculated from the daily data presented in Fig. 2. Additionally, the mean values of $\delta^{13}C$ and OC calculated for N and S winds are also compiled in Table SM2. The straight-line distance between sites 7 and 8 is about 34.5 km in a direction close to the preferential, bidirectional wind trajectory (Fig. 2). When data from the sites are aligned along that trajectory line, changes in PM_{10} emissions can be followed by using concentration changes between sampling sites. A new emitter increases OC concentration in the wind direction along the trajectory, with a corresponding change in $\delta^{13}C$ values (Fig. 5; Table SM2). Calculations of the contribution of that single emitter to the total OC emissions is based on the OC and ^{13}C mass balance (Eqs. (1) and (2)) with known (or presumed) $\delta^{13}C$ values of source total OC, and δ ^{13}C and unknown variables (OC contributions)–Appendix A.

3.2.1. *February (Late winter) data*

Site 7 had the lowest OC concentrations among all sites, especially under S winds (12 μg m^{-3}; Fig. 2; Table SM2). This finding corresponds to the marginal position of this site, away from the area where the principal emitters are located (Fig. 1). Thus, site 7 was exposed only to emissions from local traffic and coal combustion associated with domestic heating. We solved the mass balance for traffic contribution ($\delta^{13}C_{traf}$ = −26.5‰), local coal combustion (δ $^{13}C_{coal}$ −25.5 to −25.75‰) and total OC-δ $^{13}C_{tot}$ = −26‰ (c_{tot} = 12 μg m^{-3})–Appendix A.

Traffic-related PM_{10} contributions were invariably present at all OC measurements at all the sites. The OC/EC ratio at site 7 (4.3–5.7; Table SM2) differed from the value of 2–2.5 assumed for traffic emissions exclusively (Pio et al., 2011; Gorka et al., 2020). Higher OC/EC ratios at site 7 point to the additional contribution of local coal combustion to OC. The assumption that OC from automobile exhausts contributes to PM_{10} emissions throughout the year in Ostrava is supported by the yearly average based on the daily number of cars (40,000) and trucks (10,000) in the area. Garbariene et al. (2016) applied the same presumption of a constant traffic contribution to PM_{10} emissions in Vilnius, Lithuania.

According to the histograms shown on Fig. 3, another relevant contribution to PM_{10} were emissions transferred from Poland by N winds. Accordingly, site 8, at the Czech Polish border (Fig. 1), had the highest OC concentrations in winter (24.5 and 20 μg m^{-3}), and corresponding δ $^{13}C_{tot}$ values of between −24.7 and −24.8‰ (Fig. 2). After subtracting C_{traf}, we obtained (from Eq. (1) in Appendix A) between 20 and 16 μg m^{-3} for C_{coal}. The δ $^{13}C_{tot}$ values for OC transported in PM_{10} by N winds again revealed Silesian coal combustion as the main emission source. A control calculation of δ_{tot} resulted in −24.8‰. At site 8, due to

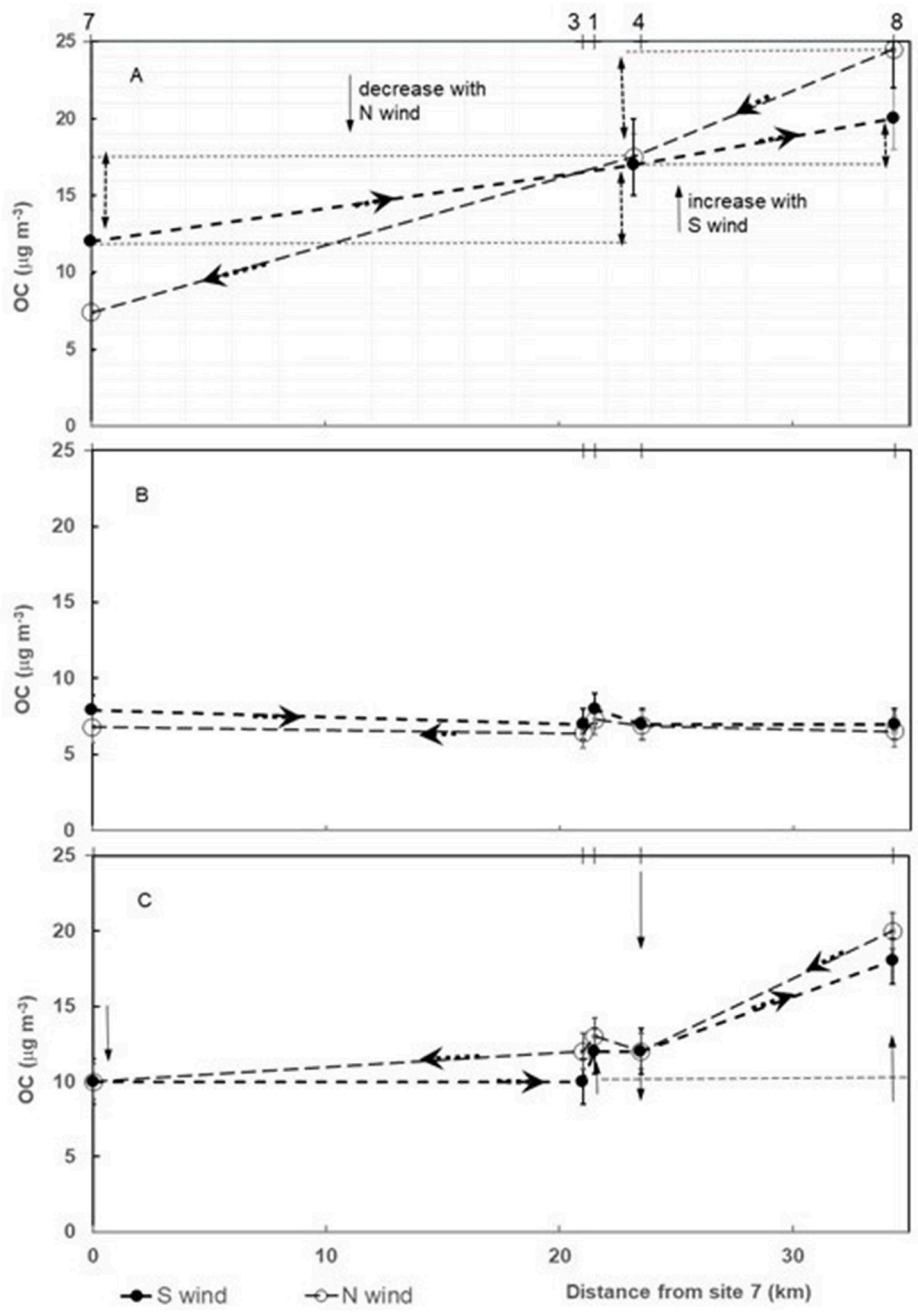

Fig. 5. Mean OC concentration of PM_{10} at the monitored sites 7, 3, 1, 4, and 8 under S and N wind flow. The black filled circles denote a South-North trajectory, and the white circles edged in gray indicate a North-South trajectory. The arrows show the direction of the wind flow. A, B, and C correspond to February, July, and December sampling. Changes in OC concentration with wind flow are highlighted. Numbers on the upper trend line correspond with the site positions along the trajectory. Error bars correspond to ± SE.

its location near the border, there was a significant reduction in the amount of pollution that originated in Poland particularly at times when S winds exhibited the highest measured wind speeds (Fig. 2).

An alternative explanation that would link the observed ^{13}C depletion of OC when S winds prevailed is aging of SOC- $\delta^{13}C$ values in winter (Wang et al., 2010; Morera-Gomez et al., 2021). But SOC contribution to OC ranges between 1.2 and 1.6 µg m^{-3} (CHMI et al., 2022). This contribution is about 10% of the estimated C_{coal} for S winds and falls within the error determined for OC concentrations (Table SM2). Importantly, a contribution of less negative $\delta^{13}C$ of SOC to $\delta^{13}C_{tot}$ can cause a negligible effect on our estimate of the polluting contribution of Silesian coal combustion under N wind conditions.

C_{tot} and δ_{tot} for site 4 is solved with a contribution $C_{coal} = 13$ µg m^{-3} with δ_{coal} −25.5‰ for S winds. Mean $\delta^{13}C_{tot}$ on site 4 differs for S- and N winds at practically the same OC concentrations (see Table SM2). Difference between $\delta^{13}C_{tot}$ for N- ($\delta^{13}C_{tot} = -25.4$‰) and S-bound winds ($\delta^{13}C_{tot} = -25.6$‰) is within the standard error value, and it is not significant.

3.2.2. *July (summer) data*

As shown in Fig. 5B (see also Table SM2), the OC concentrations measured in July were two or three times lower than those of the PM_{10} collected in February. The $\delta^{13}C$ values of OC collected on all sites were shifted by about two per mil, towards more negative values than those of $\delta^{13}C_{traf}$ (Fig. 6B). This shift likely resulted from a relatively higher contribution of biogenic material ($\delta^{13}C = -27.5$ to −28.5‰) in PM_{10} particles. The isotopic shift was measurable even at low summer OC concentrations (from 6.5 to 8 µg m^{-3}), and results from the missing contribution of winter coal combustion. The contribution of other (industrial) sources to OC concentration was low (around 1 µg m^{-3}), and can be observed on the plot of OC concentrations along the wind trajectory (site 1 on Fig. 5B). If we assume a constant automotive OC

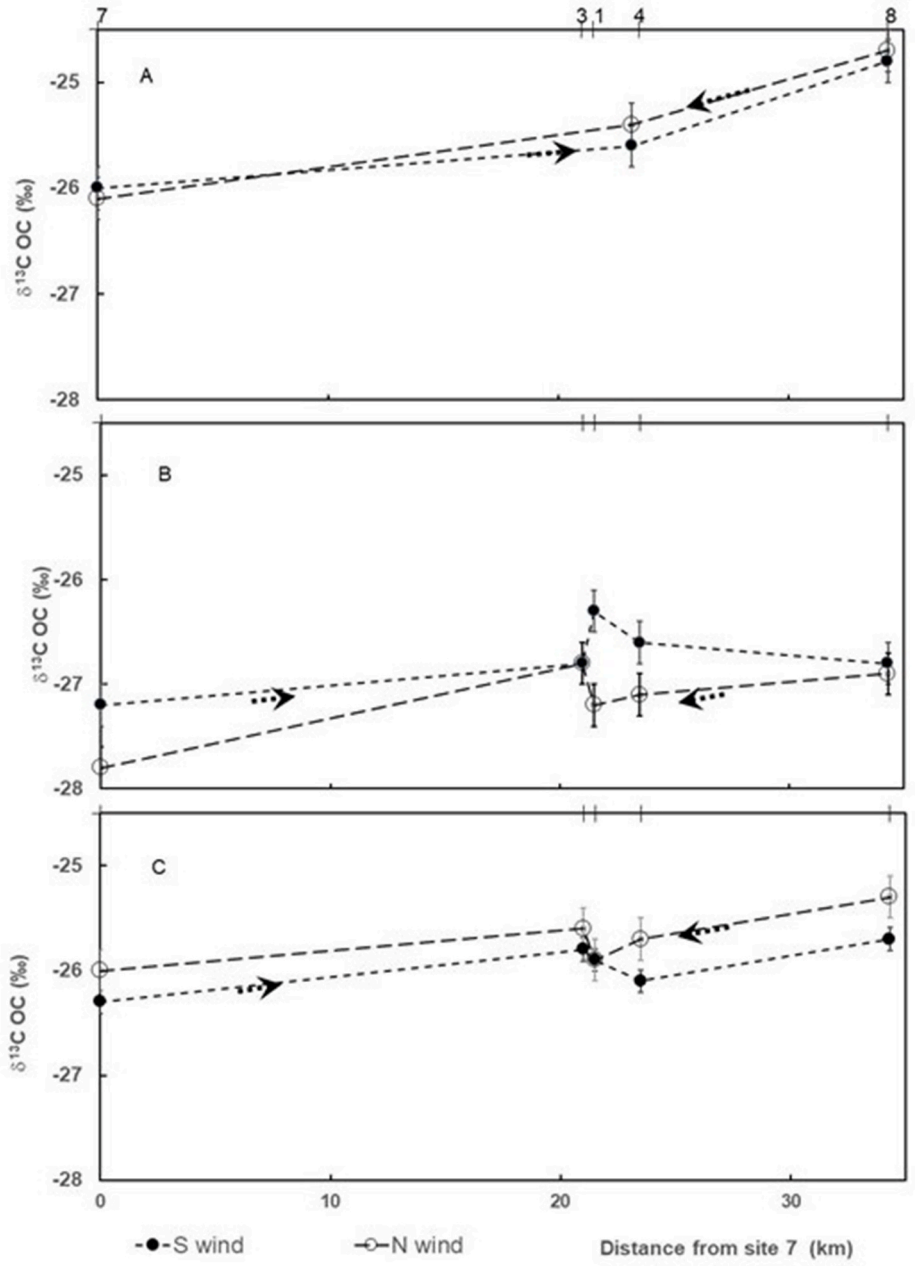

Fig. 6. Mean $\delta^{13}C$ values of PM_{10} collected at sites numbers 7, 3, 1, 4, and 8 during S and N wind flow. The black filled circles denote a South-North trajectory, and the white circles edged in gray indicate a North-South trajectory. The arrows show the direction of the wind flow. A, B, and C correspond to February, July, and December sampling. Numbers on the upper trend line correspond with the site positions along the trajectory. Error bars correspond to ± SE.

contribution, $C_{traf} = 4$ μg m^{-3}, then the biogenic contribution C_{bio} in July can be estimated at around 3 μg m^{-3}. In July, biogenic inputs accounted for 40–50% of OC in PM_{10} at all the monitored sites, with the remainder attributed to traffic inputs.

The uncertainty of the isotope mass balance calculation is large because of a relatively high contribution of SOC, 1.5–1.8 μg m^{-3}, in summer (CHMI et al., 2022). This has an unknown $\delta^{13}C$ value. While Vodicka et al. (2022) indicate a low and constant shift (+0.7‰) between the $\delta^{13}C$ values of OC and WSOC, other studies presented a higher difference of between 2 and 3‰ (Dai et al., 2015; Morera-Gomez et al., 2021). Cao et al. (2011) reported negative SOC (−30‰) formed from automotive emissions in summer. Such a difference could change our mass balance calculation results in summer by about 20–25%. Negative $\delta^{13}C$ of SOC would replace part of the biogenic contribution which would then be lower than the calculated ~3 μg m^{-3}. The influence of SOC on sources apportionment in July is probably as low as 1.5 μg m^{-3} as determined from site 8, but it was not estimated for all other sites.

3.2.3. *December (Early winter) data*

Data collected in December closely resemble that from February (Table SM2). The southern locales at the monitored area had mean OC concentrations of 10 μg m^{-3}, mean $\delta^{13}C_{tot}$ ranging from −26 to −26.3‰, and with slightly higher isotope values observed under the influence of S winds. These values are solved with a mass balance involving 4 μg m^{-3} attributable to automotive contributions ($\delta_{traf} = -26.5$‰), and 6 μg m^{-3} to coal combustion ($\delta_{coal} = -25.7$‰). Concentrations of OC increased at sites near to local emission sources (1, 3 and 4) from 10 μg m^{-3} to up to 13 μg m^{-3}. The observed increase in OC concentration is consistent with an additional contribution of local industrial emissions ($\delta^{13}C$ ~ −25.7‰). The northern locales of the monitored area had the highest

OC concentrations (Fig. 5C) of about 18 μg m^{-3} transported by S winds and 20 μg m^{-3} for N winds, respectively. The corresponding mean values of PM_{10} are $\delta^{13}C = -25.7‰$ for S winds, indicative of an automotive emissions contribution of about 4 μg m^{-3}, and with some 14 μg m^{-3} attributable to local industrial emissions. N winds (mean $\delta^{13}C = -25.3‰$) bring an additional contribution (8–9 μg m^{-3}) of coal combustion emissions originating in Polish Silesia (Fig. 6C).

The distribution, or apportionment of OC sources across the monitored sites (Fig. 7- 8) shows that in addition to PM_{10} deposition from vehicle exhausts, Ostrava coal combustion, biogenic inputs, and Silesian coal combustion together contributed significantly in the study area. When the OC contributions under north (Figs. 7A and 8A) and south (Figs. 7B and 8B) wind directions are compared, significant differences in the contribution of Silesian combustion emerge. Accordingly, under S wind conditions, emissions from local industry were the dominant source of OC in PM_{10} at the monitored area, accounting for from 60 to 70%. Except for site 8, most of the emissions originated from Polish Silesia. Under N wind conditions, at site 8 the combustion of Silesian coal can be linked to 80% of OC in PM_{10} in February, but only by 40% in December. The decrease of the Silesian contribution in December originates from generally lower emissions (see Table SM2). Coal use and combustion were therefore the dominant emitters in early winter (55–74%), followed by traffic inputs. The contribution of biogenic inputs was much lower.

Two recent studies analyzing $\delta^{13}C$ of OC in PM were conducted near to the Czech border in Lower Silesia, Poland. In the first, Zimnoch et al. (2020) analyzed the contributions of various sources to the carbonaceous fraction of $PM_{2.5}$ in Krakow. In their study—conducted in summer, biogenic, traffic, and coal combustion sources accounted for approximately 52%, 40%, and 7% of all OC emissions, respectively. In winter, their estimates on contributions of biogenic, coal combustion, and traffic sources to OC emissions were 54%, 37%, and 9%, respectively. The disparate apportionment in their study compared to ours is likely due to a higher contribution of biogenic OC in winter, probably due to more intensive biomass combustion. The population of Krakow is about four times larger than that of Ostrava, and the monitored area in their study was about twice as large as ours.

In addition, there is no heavy industry in Krakow. In the second study, Gorka et al. (2020) analyzed sources of OC in PM_{10} in the Lower Silesian Voivodeship (total area: approximately 19,000 km^2) based on

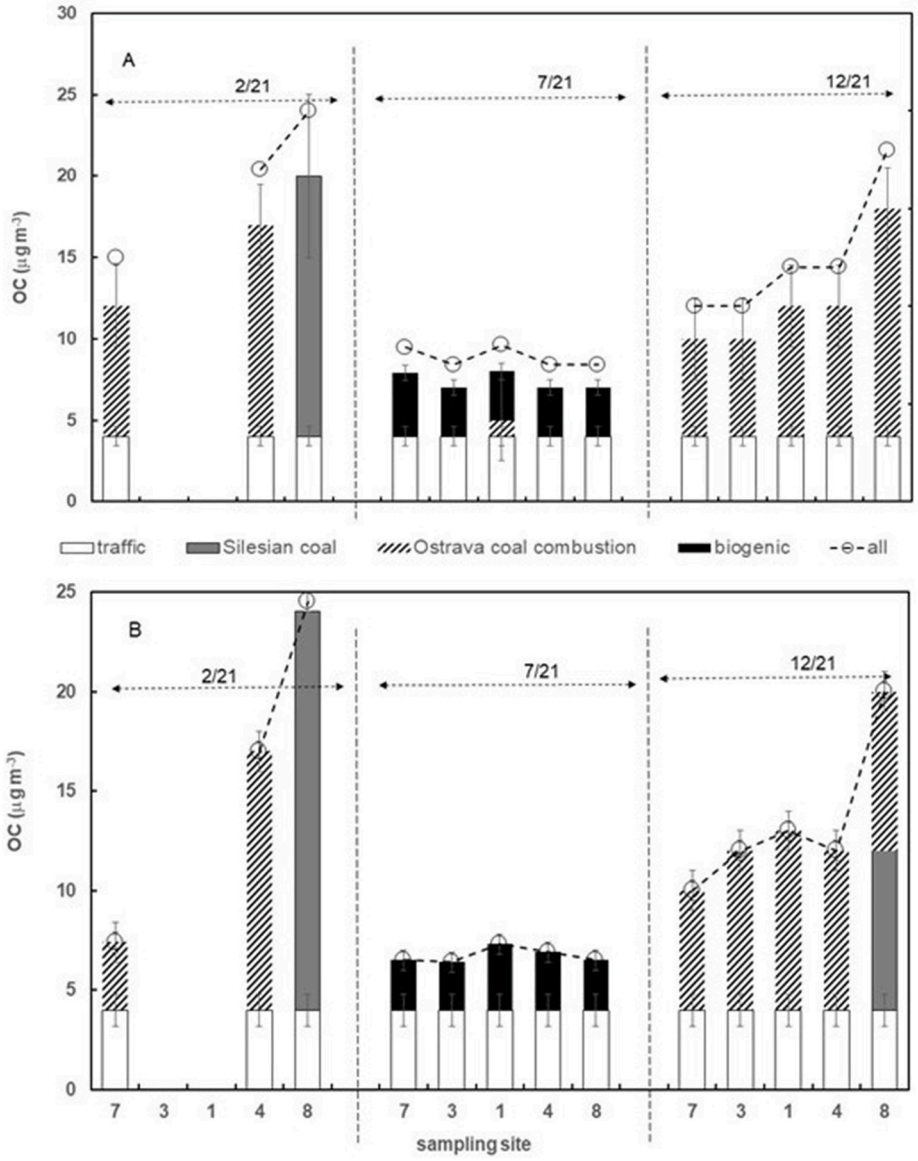

Fig. 7. Apportionment of sources of PM emissions represented by the OC concentration under southern wind (A) and northern wind (B) conditions. The sampled sites are presented on the x axis, and the OC concentrations are on the y axis.

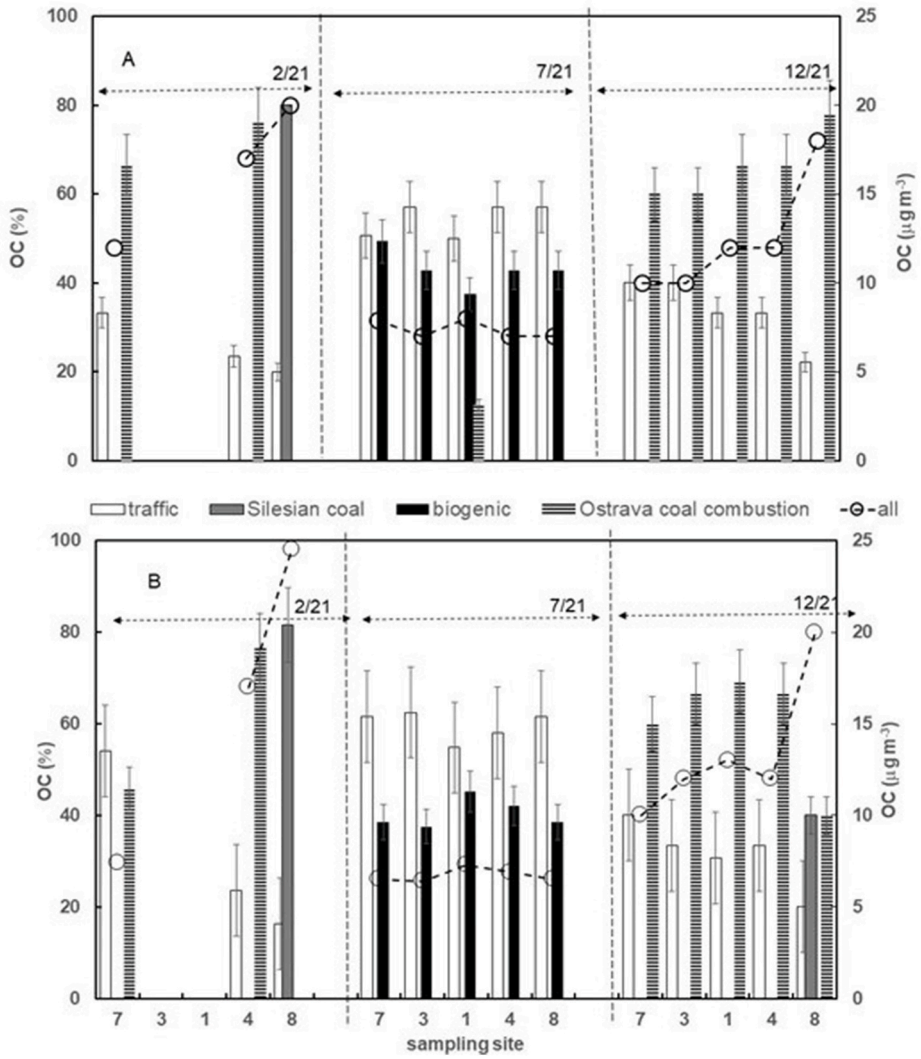

Fig. 8. Apportionment of sources of PM emissions represented as the percent of the total OC concentration under southern wind (A) and northern wind (B) conditions. The sampled sites are presented on the x-axis, and the total OC concentration is presented on the secondary y-axis.

OC, EC, $\delta^{13}C$, and ^{14}C data. In their study, coal combustion was the dominant source of PM_{10} emissions in the industrial region (OC range: 5–74 μg m^{-3}) in the winter season, and traffic and biogenic sources were the dominant sources during the summer (2–20 μg m^{-3}). With an increase in the size of the area monitored, heterogeneity in PM_{10} emissions increased. The range of variation in the concentrations of OC in PM_{10} also increased.

3.3. The effect of a temperature inversion

During unusually temperate winter days, when a warm air mass sits above a colder one, pollutants that would be typically blown away are held close to ground, which result in particularly unhealthy air conditions. In the present study, such a phenomenon, termed a temperature inversion, was recorded between 26 and 27th December 2021. The inversion was linked to low-lying clouds with no airflow. The lack of airflow had a significant impact on PM_{10} accumulation, and the OC concentrations at the filters were two-fold higher than mean values (Table 2). For that specific event, Fig. 9 shows the relation between OC concentrations and $\delta^{13}C$ values (Keeling plot). Site 1 showed values that can be directly extrapolated to those of the nearby source value ($\delta^{13}C = -25.8‰$). The other sites lay on the mixing-line with two end-members, one with the $\delta^{13}C$ value of −24.3‰ and another of-25.0‰. The end-members of this mixing-line correspond to contributions from combustion of Silesian and Ostrava coals. The $\delta^{13}C$ value of −25.8‰, which is the extrapolated source value at site 1, is close to the mean $\delta^{13}C$ value of the local coal (Fig. 3).

Table 2
OC contents (in weight %) and $\delta^{13}C$ values of PM_{10} on QF filters from the monitored sites on 26 and 27 December 2021.

Site		1	3	4	7	8
26.12.2021	$\delta^{13}C$ (‰)	−25.1	−24.6	−24.6	−24.8	−24.2
PM_{10} (71 μg m^{-3})	OC (%)	24.9	17.7	20.5	13.1	17.8
27.12.2021	$\delta^{13}C$ (‰)	−25.0	−24.6	−24.7	−24.6	−24.5
PM_{10} (124 μg m^{-3})	OC (%)	20.1	14.9	16.1	18.7	14.9

3.4. Emission deposition on soil

Although coal mined at the Most basin has recently been used in domestic heating in Ostrava, locally abundant coal is more extensively used. Thus, we can assume that PM_{10} from coal combustion and their $\delta^{13}C$ values remained mostly unchanged throughout the years. We can also assume that long-lasting PM_{10} deposition in soils at, or adjacent to our sites originated from the tracked emitters. To analyze soil BC and its $\delta^{13}C$, we sampled the upper layers of non cultivated soils from an open

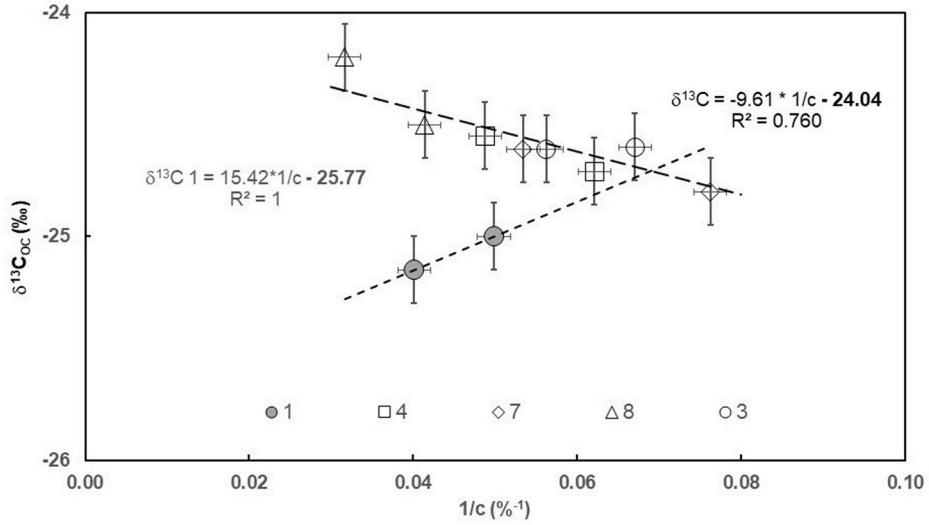

Fig. 9. Plot of the relationship between carbon content and $\delta^{13}C$ values of PM emissions at the sampling sites on 26 and 27 December 2021.

area (i.e., without trees, roads or cultivation; just under grass) at eight sites (Fig. 1). The same sampling procedure was used before for tracking antimony and arsenic in PM_{10} deposition (Dousova et al., 2020). The resulting data are presented in Table 3. The soil OC and BC data are shown in Fig. 10.

The measured $\delta^{13}C$ values in OC and BC were markedly different. Specifically, OC $\delta^{13}C$ values (−27.5 to −29‰) covered a wide range of C3 plants. In contrast, the BC $\delta^{13}C$ values (−24.5 to −25.5‰) covered a much narrower range corresponding to PM_{10} emissions from a mix of Silesian hard and local Ostrava coals. As in Fig. S1 and Fig. 9, the $\delta^{13}C$ value of the dominant source of deposition was estimated from a Keeling plot (Supplement Fig. S2). The extrapolated $\delta^{13}C$ value in Fig. S2 (−24.5‰) corresponds to that of Silesian coal. This finding is consistent with data presented in Table SM2 and Figs. 7B and 8B, where emissions during wintertime, under north winds, were the highest at site 8 and formed the majority of long-term PM_{10} deposition (e.g., Zimnoch et al., 2020). In addition, the $\delta^{13}C$ values of OC measured under a temperature inversion (Fig. 9) were strongly affected by inputs from Silesian coal combustion (−24.5‰).

4. Summary and conclusions

The aim of this study was to identify major sources of PM_{10} emissions in the industrial city of Ostrava and their contributions to total PM_{10} pollution with respect to seasonal, climatic, and airflow conditions. Airflow at the monitored sites is in a South-North or North-South direction 60–80% of the time. We calculated the contributions of single emitters to PM_{10} emissions based on OC and ^{13}C mass balance equations, and with several assumptions:

Table 3
Soil OC and BC contents and $\delta^{13}C$ values. The mean value and SE were calculated from the measurements of three samples.

Site	Soil OC				Soil BC			
	$\delta^{13}C$ (‰)	±SE	C wt. %	±SE	$\delta^{13}C$ (‰)	±SE	C wt. %	±SE
1	−28.85	0.81	3.94	0.64	−24.81	0.11	1.01	0.09
2	−29.50	0.32	3.25	0.49	−24.67	0.22	0.90	0.12
3	−29.89	0.15	2.96	0.44	−24.98	0.15	0.32	0.08
4	−28.79	0.19	2.02	0.35	−24.87	0.24	0.45	0.05
5	−27.50	0.46	4.05	0.44	−24.78	0.16	0.79	0.07
6	−28.47	0.15	2.85	0.31	−24.85	0.18	0.45	0.04
7	−28.72	0.16	5.19	0.44	−25.37	0.19	0.33	0.04
8	−28.58	0.61	5.33	0.54	−24.83	0.11	0.59	0.14

(i) the $\delta^{13}C$ values of sources are constant and different from each other, and measurable changes in PM_{10} arise only by mixing with other sources
(ii) the $\delta^{13}C$ values of sources can be estimated from extrapolated values in the Keeling graphs, and can be related to values from the literature or measurable at potential point sources
(iii) PM_{10} emissions from traffic inputs are constant in a given study area and do not change during the year, as supported by automotive emission data (cars and trucks) in the area
(iv) Biogenic inputs are significant only during the summer growing season. Wood combustion in the wintertime is not frequent enough to be a significant source in the OC balance.

Measured OC concentrations are four to eight times higher than EC. Although some mean $\delta^{13}C$ data of OC and EC are different, which implies additional mixing of OC sources, we preferred more abundant and precise OC data against EC for isotope mass balance calculation. Absence of ^{13}C data of SOC sources (SOC concentration were 1.2–1.6 μg m^{-3}) added uncertainty to the evaluation of summer data with low OC concentration (6–8 μg m^{-3}) and ^{13}C depleted OC. It is probable that biogenic emissions were not as high in summer, as we estimated.

Winter emissions were more concentrated in OC and the effect of the absence of $\delta^{13}C$ SOC data is comparable with the overall uncertainty of the mass balance calculation. The exception was the S wind condition in February 2021, when our estimate of source apportionment also included contributions from the north. An alternative explanation for less negative $\delta^{13}C$ OC values would be a contribution of aged SOC particles, which would resemble part of the Silesian coal contribution in the isotope mass balance calculation implemented here.

Based on the results of the present study, we conclude that tracking sources of PM_{10} pollution using OC mass determinations together with $\delta^{13}C$ analysis can be applied even on small areas with many sources. The method could allocate corporate carbon accounting. The $\delta^{13}C$ values of sources were not so different and the linking of data to airflow trajectory simplified tracking of emission sources along this trajectory. A variable airflow rate introduced a large variability in OC data and a significant standard error in the mass OC estimate. In contrast, the variability of $\delta^{13}C$ values with the variable airflow rate was low, which resulted in a low standard error of the $\delta^{13}C$ estimate.

As hypothesized, the EC (or BC in soil), is a very stable part of PM emissions and the deposition of pollution sources can be traced in soils. Long-term combustion and deposition of the same coals in the studied area created a $\delta^{13}C$ record of BC in topsoil, which was quite different from the soil OC $\delta^{13}C$ data, but in agreement with the sources $\delta^{13}C$ data.

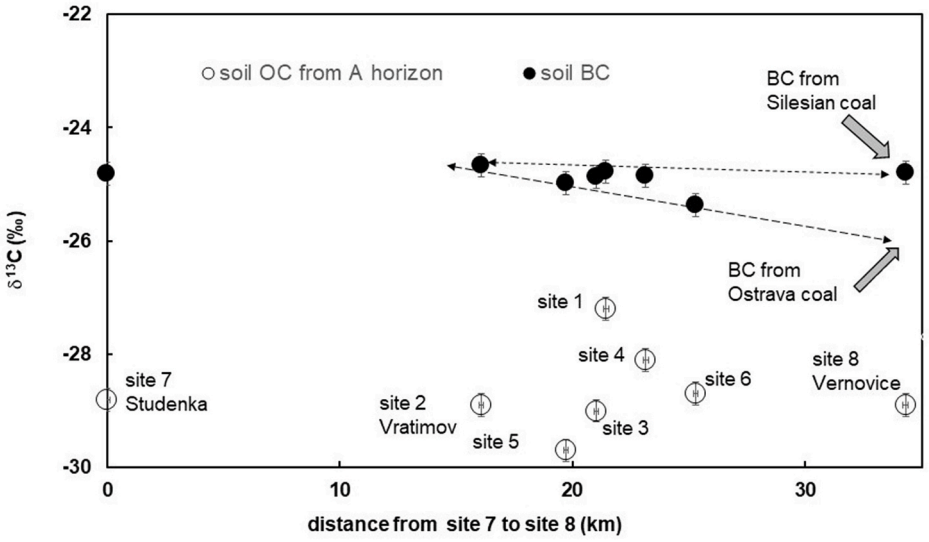

Fig. 10. $\delta^{13}C$ values of OC (empty circles) and BC (black-filled circles) in topsoil from the sampling sites.

CRediT authorship contribution statement

Frantisek Buzek: evaluated data and prepared the paper. **Bohuslava Cejkova:** analyzed carbon isotopes, elemental and OC, EC measurements. **Ivana Jackova:** analyzed carbon isotopes, elemental and OC, EC measurements. **Radim Seibert:** contributed to text revisions, control of OC and EC data and managed field campaign. **Jan Curik:** realized all sampling in the field (PM and soils samples) together with sample logistic. **Frantisek Veselovsky:** realized all sampling in the field (PM and soils samples) together with sample logistic. **Daniel A. Petrash:** analyzed data, prepared statistics.

Declaration of competing interest

The authors declare that they have no known competing financial interests or personal relationships that could have appeared to influence the work reported in this paper.

Data availability

Data will be made available on request.

Acknowledgments

The authors wish to thank Lenka Buresova for her technical and analytical support. The Associate Editor, C.J. Hennigan, and two anonymous reviewers are gratefully acknowledged for their useful and constructive comments that significantly improved the quality of the manuscript. This study was supported by the Czech Science Foundation Project No. 19-04682S and by the Technological Agency of the Czech Republic (project SS 020 30031).

Appendix B. Supplementary data

Supplementary data to this article can be found online at https://doi.org/10.1016/j.atmosenv.2022.119556.

Appendix A

Two linear equations (Eqs. A.1, A.2) have a solution for two variables. The solution for more variables is to reduce the number of variables by linear combination with C_{tot} (parametric solution), or by the approximative estimate of any other variable.

$$C_{tot} = C_{coal} + C_{traf} \quad (A.1)$$

$$C_{tot} * \delta_{tot} = C_{coal} * \delta_{coal} + C_{traf} * \delta_{traf} \quad (A.2)$$

The unknown variable C_{coal} is substituted by the expression "C_{tot} - C_{traf}" in Eq. A.2.

$$C_{tot} * \delta_{tot} = C_{traf} * \delta_{traf} + \delta_{coal} * (C_{tot} - C_{traf}) \quad (A.3)$$

After factorization, we get

$$C_{traf} = C_{tot} * (\delta_{tot} - \delta_{coal}) (\delta_{traf} - \delta_{coal})^{-1} \quad (A.4)$$

with solution $C_{tot} = 12$ μg m^{-3}, $C_{traf} = 4 =$ μg m^{-3} and $C_{coal} = 8$ μg m^{-3}.

A control calculation is $\delta_{tot} = (4* -26.5 + 8*-25.75)/12 = -26‰$. This control calculation of $\delta_{tot\ constrains}$ the sensitivity of the balance method to uncertainty in OC concentration. For example, C_{traf} would be (4 + SE) = 6 μg m^{-3}, a $\delta_{tot} = -26.1‰$ (i.e., 1 SE ≡ 0.1‰).

References

Asa-Awuku, A., Moore, R.H., Nenes, A., Bahreini, R., Holloway, J.S., Brock, C.A., et al., 2011. Airborne cloud condensation nuclei measurements during the 2006 Texas air quality study. J. Geophys. Res. Atmos. 116, D11201 https://doi.org/10.1029/2010/JD014874.

Buzek, F., Cejkova, B., Jackova, I., Gerslova, E., Mach, K., Lhotka, M., Curik, J., Veselovsky, F., 2022. Secondary processes on coal deposits change the emission of greenhouse gases. Int. J. Coal Geol. 262, 104102 https://doi.org/10.1016/j.coal.2022.104102.

Cao, J., Chow, J.C., Tao, J., Lee, S., Watson, J.G., Ho, K., Wang, G., Zhu, Ch, Han, Y., 2011. Stable carbon isotopes in aerosols from Chinese cities; Influence of fossil fuels. Atmos. Environ. 45, 1359–1363. https://doi.org/10.1016/j.atmosenv.2010.10.056.

Cavalli, F., Viana, M., Yttri, K.E., Genberg, J., Putuaud, J.-P., 2010. Toward a standardized thermal-optical protocol for measuring atmospheric organic and elemental carbon: the EUSAAR protocol. Atmos. Meas. Tech. 3, 79–89. www.atmos-meas-tech.net/3/79/2010/.

Chow, J.C., Watson, J.G., Chen, L.-W., Rice, J., Frank, N.H., 2010. Quantification of PM2.5 organic carbon sampling artifacts in US networks. Atmos. Chem. Phys. 10, 5223–5239. https://doi.org/10.5194/acp-10-5223-2010.

CHMI, Seibert, R., Volna, V., Hladky, D., Krejci, B., 2022. Sources of Atmospheric Pollution and Their Distribution through the Main Corridor of North Moravia. *Suppl. 1 Identification of the Sources*. Czech Hydrometeorological Institute, Ostrava, p. 21 pp (in Czech).

Dai, S., Bi, X., Chan, L.Y., He, J., Wang, B., Wang, X., Peng, P., Sheng, G., Fu, J., 2015. Chemical and stable carbon isotopic composition of PM2.5 from on-road vehicle emissions in the PRD region and implications for vehicle emission control policy. Atmos. Chem. Phys. 15, 3097–3108. https://doi.org/10.5194/acp-15-3097-2015.

Dienes, P., 1980. The isotopic composition of reduced organic carbon. In: Fritz, P., Fontes, J.C. (Eds.), Handbook of Environmental Isotope Geochemistry. Vol. I, The Terrestrial Environment, A. Elsevier Scientific Publishing Company, New York, pp. 329–406.

Dousova, B., Lhotka, M., Buzek, F., Cejkova, B., Jackova, I., Bednar, V., Hajek, P., 2020. Environmental interaction of antimony and arsenic near busy traffic nodes. Sci. Total Environ. 702, 134642 https://doi.org/10.1016/j.scitotenv.2019.1346420048-9697.

Garbariene, I., Sapolaite, J., Garbaras, A., Ezerinskis, Z., Pocevicius, M., Krikscikas, L., Plukis, A., Remeikis, V., 2016. Origin identification of carbonaceous aerosol particles by carbon isotope ratio analysis. Aerosol Air Qual. Res. 16, 1356–1365. https://doi.org/10.4209/aaqr.2015.07.0443.

Gorka, M., Kosztowniak, E., Lewandowska, A.U., Widory, D., 2020. Carbon isotope composition and TC/OC/EC levels in atmospheric PM10 from lower Silesia (SW Poland): spatial variation, seasonality, sources and implications. Atmos. Pollut. Res. 11, 1099–1114. https://doi.org/10.1016/j.apr.2020.04.003.

Gustafsson, O., Bucheli, T.D., Kukulska, Z., Andersson, M., Largeau, C., Rouyand, J.-N., Reddy, Ch M., Egligton, T.I., 2001. Evaluation of a protocol for the quantification of black carbon in sediments. Global Biogeochem. Cycles 15, 881–890. https://doi.org/10.1029/2000GB001380.

He, G., Ma, J., He, H., 2018. Role of carbonaceous aerosols in catalyzing sulfate formation. ACS Catal. 8, 3825–3832. https://doi.org/10.1021/acscatal.7b04195.

Jancik, P., Pavlikova, I., Bitta, J., Hladky, D., Lach, K., 2013. Air Silesia, Atlas of Ostrava Atmosphere. Technical University of Ostrava, Ostrava (in Czech).

Jones, A.M., Harrison, R.M., 2005. Interpretation of particulate elemental and organic carbon concentrations at rural, urban and kerbside sites. Atmos. Environ. 39, 7114–7126. https://doi.org/10.1016/j.atmosenv.2015.08.087.

Keeling, C.D., 1961. The concentration and isotopic abundance of carbon dioxide in rural and marine air. Geochem. Cosmochim. Acta 24, 277–298.

Klimont, Z., Kupiainen, K., Heyes, Ch, Purohit, P., Cofala, J., Rafaj, P., Borken-Kleefeld, J., Schöpp, W., 2017. Global anthropogenic emissions of particulate matter including black carbon. Atmos. Chem. Phys. 17, 8681–8723. https://doi.org/10.5194/acp-17-8681-2017.

Komada, T., Anderson, M.A., Dorfmeier, C.L., 2008. Carbonate removal from coastal sediments for the determination of organic carbon and its isotopic signatures, δ13C and Δ14C: comparison of fumigation and direct acidification by hydrochloric acid. Limnol Oceanogr. Methods 6, 254–262. https://doi.org/10.4319/lom.2008.6.254, 2008.

Lewan, M.D., Kotarba, M.J., 2014. Thermal-maturity limit for primary thermogenic –gas production from humic coals as determined by hydrous pyrolysis. AAPG Bull. 98, 2581–2610. https://doi.org/10.1306/06021413204.

Liu, J., Mo, Y., Ding, P., Li, J., Shen, C., Zhang, G., 2018. Dual carbon isotopes (C-14 and C-13) and optical properties of WSOC and HULIS-C during winter in Guangzhou, China. Sci. Total Environ. 633, 1571–1578. https://doi.org/10.1016/j,scitotenv.2018.03.293.

Lopez-Veneroni, D., 2009. The stable carbon isotope composition of PM2.5 and PM10 in Mexico City metropolitan area air. Atmos. Environ. 43, 4491–4502. https://doi.org/10.1016/j.atmosenv.2009.06.036.

Morera-Gomez, Y., Cong, Z., Widory, D., 2021. Carbonaceous fractions contents and carbon stable isotope compositions of aerosols collected in the atmosphere of montreal (Canada): seasonality, sources, and implications. Front. Environ. Sci. 9, 622521, 10.33898fenvs.2021.622521.

Pio, C., Cerqueira, M., Harrison, R.M., Nunes, T., Mirante, F., Alves, C., Oliveira, C., Sanchez de la Campa, A., Artinano, B., Matos, M., 2011. OC/EC ratio observation in Europe: Re-thinking the approach for apportionment between primary and secondary organic carbon. Atmos. Environ. 45, 6121–6132. https://doi.org/10.1016/j.atmosenv.2011.08.045.

Szidat, S., Jenk, T.M., Gaaggler, H.W., Synal, H.-A., Fisseha, R., Baltespergere, U., et al., 2004. Source apportionment of aerosols by 14C measurements in different carbonaceous particle fractions. Radiocarbon 46, 475–484. https://doi.org/10.1017/S0033822200039783.

Vodicka, P., Kawamura, K., Schwarz, J., Zdimal, V., 2022. Seasonal changes in stable carbon isotopic composition in the bulk aerosol and gas phases at a suburban site in Prague. Sci. Total Environ. 803, 149767 https://doi.org/10.1016/j.sci.tot.env.2021.149767.

Wang, G., Xie, M., Hu, S., Gao, S., Tachibana, E., Kawamura, K., 2010. Dicarboxylic acids, metals and isotopic composition of C and N in atmospheric aerosols from inland China: implications for dust and coal burning emission and secondary aerosol formation. Atmos. Chem. Phys. 10, 6087–6096. https://doi.org/10.5194/acp-10-6087-2010.

Widory, D., 2006. Combustiles, fuels and their combustion products: a view through carbon isotopes. Combust. Theor. Model. 10 https://doi.org/10.1080/13647830600720264, 831-541.

Zimnoch, M., Samek, L., Furman, L., Styszko, K., Skiba, A., Gorczyca, Z., Galkowski, M., Rozanski, K., Konduracka, E., 2020. Application of natural carbon isotopes for emission source apportionment of carbonaceous particulate matter in urban atmosphere: a case study from Krakow, southern Poland. Sustainability 12, 5777. https://doi.org/10.3390/su12145777.